Chemistry–A European Journal
Full Paper
doi.org/10.1002/chem.202000005
Chemistry Europe
European Chemical Societies Publishing

Organic Electronics

A Self-Assembled Small-Molecule-Based Hole-Transporting Material for Inverted Perovskite Solar Cells

Miriam Más-Montoya[+],[a] Paula Gómez[+],[a] David Curiel,*[a] Ivan da Silva,[b] Junke Wang,[c] and René A. J. Janssen*[c, d]

Abstract: Hybrid organic–inorganic perovskite solar cells have recently emerged as one of the most promising low-cost photovoltaic technologies. The remarkable progress of perovskite photovoltaics is closely related to advances in interfacial engineering and development of charge selective interlayers. Herein, we present the synthesis and characterization of a fused azapolyheteroaromatic small molecule, namely anthradi-7-azaindole (**ADAI**), with outstanding performance as a hole-transporting layer in perovskite solar cells with inverted architecture. Its molecular arrangement, induced by hydrogen-bond-directed self-assembly, favors a suitable morphology of the perovskite layer, reducing the effects of recombination as revealed by light intensity dependence, photoluminescence, and electroluminescence studies.

Introduction

The application of organic–inorganic metal halide perovskites as photoactive materials in photovoltaic devices has marked a milestone in the development of thin film solar cells.[1] There are not many precedents in the recent scientific research on photovoltaics that have experienced such a remarkable evolution in just a decade of studies.[2] Essentially, the outstanding performance of metal halide perovskite materials in solar cells arises from their excellent light-harvesting properties,[3] ambipolar charge transport ability,[4] high charge carrier mobility,[5] long charge diffusion lengths,[6] and low trap densities,[7] amongst others.[8] These features enhance the potential of perovskite-based photovoltaics as a low-cost technology for clean and renewable energy production, reaching higher efficiencies than those of some of the commercially available solar cells.[9] Many efforts are currently devoted to improve the device performance, aiming at different aspects which involve the optimization of the fabrication protocols,[10] the power conversion efficiency (PCE), and the device stability.[11] In this regard, much attention has been paid to the device architecture. The concept of a planar heterojunction has been successfully adapted to perovskite solar cells, benefitting from the knowledge acquired in organic photovoltaics, particularly in the case of the *p*-i-n, or inverted, device architecture.[12] In *p*-i-n solar cells, a hole-transporting layer (HTL) is deposited on a transparent front electrode, followed by the perovskite semiconductor, and an electron transporting layer (ETL) with a metal back electrode atop. Compared to the n-i-p, or conventional, configuration, the inverted architecture has a larger prospective of commercialization since it can be easily manufactured from solution at much lower temperatures and, in consequence, at reduced costs.[13]

The implementation of interfacial layers in the device structure offers the possibility of improving different aspects of the solar cell performance such as selective charge transport, active layer protection, and control of the perovskite morphology.[14] Consequently, a significant part of the progress on perovskite solar cells is intimately linked to the development of new selective interlayer materials.[15] As far as organic HTLs are concerned, many interesting materials, both small molecules and polymers, have been reported.[16] As a consequence of its widespread application in organic electronics, poly(3,4-ethylenedioxythiophene):poly(styrenesulfonate) (PEDOT:PSS) is often used as HTL in *p*-i-n perovskite solar cells. Nevertheless, its known drawbacks such as hygroscopicity and acidity, imply that alternatives to PEDOT:PSS are desired.[17]

In this contribution we present the synthesis and characterization of a novel molecular material, anthradi-7-azaindole (**ADAI**), and its successful incorporation as HTL in metal halide

[a] *Dr. M. Más-Montoya,[+] P. Gómez,[+] Dr. D. Curiel*
Multifunctional Molecular Materials
Department of Organic Chemistry, Faculty of Chemistry
University of Murcia
Campus of Espinardo, 30100 Murcia (Spain)
E-mail: davidcc@um.es

[b] *Dr. I. da Silva*
ISIS Facility, STFC Rutherford Appleton Laboratory
Chilton, Oxfordshire OX110QX (United Kingdom)

[c] *J. Wang, Prof. R. A. J. Janssen*
Molecular Materials and Nanosystems, Institute for Complex Molecular Systems
Eindhoven University of Technology
P.O. Box 513, 5600 MB Eindhoven (The Netherlands)
E-mail: r.a.j.janssen@tue.nl

[d] *Prof. R. A. J. Janssen*
Dutch Institute for Fundamental Energy Research
De Zaale 20, 5612 AJ Eindhoven (The Netherlands)

[+] *These authors contributed equally to this work.*

Supporting information and the ORCID identification number(s) for the author(s) of this article can be found under: https://doi.org/10.1002/chem.202000005.

perovskite solar cells. Bearing in mind the critical role that the material nanostructure plays in organic electronics, we developed a convenient procedure of two steps only to regiospecifically synthesize this fused polyheteroaromatic system, which was rationally designed to create a material that can spontaneously self-assemble to enhance the molecular organization in the solid state.[18] The new **ADAI** molecule has a centrosymmetric structure that includes complementary hydrogen-bond donor and acceptor sites in the conjugated structure. These sites are strategically oriented to promote the self-organization of the material leading to a hydrogen-bond-directed ribbon-like supramolecular assembly, which results in π–π stacked molecular ribbons that present a favorable three-dimensional ordering for a hole-transporting interfacial layer. Other properties such as low synthetic cost, transparency to the visible range of the solar spectrum and thermal robustness reinforce the potential of **ADAI** as an excellent HTL candidate for perovskite photovoltaic devices. In fact, devices based on **ADAI** as HTL and the common methylammonium lead triiodide ($CH_3NH_3PbI_3$) perovskite achieved a maximum power conversion efficiency over 16%. The characterization of the HTL and the solar cells indicates that **ADAI** modifies the grain boundaries of the perovskite deposited on top and reduces bulk and interfacial charge recombination losses compared to PEDOT:PSS.

Results and Discussion

Compound **ADAI** was synthesized in a good overall yield following the two-step procedure outlined in Scheme 1. 1,5-Diaminoanthracene, **1**, was synthesized according to a previously reported protocol.[19] A palladium-catalyzed Buchwald–Hartwig cross-coupling reaction[20] between **1** and 2,3-dichloropyridine afforded the *N*-arylated intermediate **2**. This was subsequently cyclized via a regiospecific intramolecular photochemical reaction through positions 2 and 6 of the anthracene core to isolate **ADAI** in almost quantitative yield.[21] The identity and purity of every compound was confirmed by the common spectroscopic techniques and high resolution mass spectrometry. Further details can be found in the Experimental Section and in Figures S1–S4 (Supporting Information). The estimated synthetic cost of **ADAI** is only 26 € g^{-1} (Table S1).[22] This material is much cheaper than most of the commercially available HTLs which are commonly used in photovoltaic devices (e.g. Spiro-MeOTAD: 270–324 € g^{-1}, PTAA: 499–1175 € g^{-1}). The reduced price of **ADAI** considerably reinforces the commercial viability of our new material.

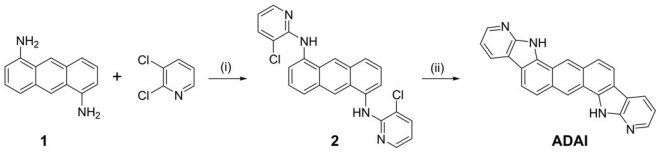

Scheme 1. Synthesis of **ADAI**: (i) *rac*-BINAP, $Pd(OAc)_2$, *t*BuOK, 1,4-dioxane (68%); (ii) *t*BuOK, DMSO, *hν* (96%).

The thermal properties of **ADAI** were investigated by thermogravimetric analysis (TGA) and differential scanning calorimetry (DSC) (Figure S5, Supporting Information). A degradation temperature as high as 496 °C (corresponding to a 5% mass loss) was detected in the TGA. The DSC thermogram did not reveal any signal that could be ascribed to glass, melting, or crystallization transitions within the scanned temperature range (25–395 °C). The observed thermal robustness of **ADAI** is a highly desirable property for materials applied in optoelectronic devices to ensure its morphological stability under device operation conditions and application via thermal sublimation.

The UV/vis absorption spectrum of **ADAI** was recorded in dimethylformamide (DMF) solution and in solid thin films (Figure 1). The absorption bands are mostly located in the UV region, showing a low-energy band located at 420 nm and a more intense peak at 337 nm. The spectrum measured for a thin film resembles that in solution but is bathochromically shifted, broader and has less-resolved bands as a consequence of the intermolecular interactions occurring in the solid state. A relatively wide optical band gap (E_g) of 2.68 eV was estimated from the onset of the lowest energy band in the thin film. The fact that **ADAI** is virtually transparent to the visible radiation makes it suitable to work as interfacial material in a solar cell.

Ultraviolet photoelectron spectroscopy (UPS) on a thermally evaporated layer of **ADAI** on indium tin oxide (ITO) gave an ionization potential of 5.04 ± 0.05 eV (Figure S6, Supporting Information), which is similar to that of PEDOT:PSS (5.06 eV).[23] Accordingly, the electronic structure of **ADAI** can be considered as suitable to selectively extract holes from a perovskite layer, where free charge carriers are generated instantaneously upon illumination.

The charge transport properties of **ADAI** layers were evaluated in single carrier devices by analyzing the space charge limited current (Figure S7, Supporting Information).[24] The hole mobility (1.1×10^{-4} $cm^2 V^{-1} s^{-1}$) makes **ADAI** a suitable semiconducting material to be employed as HTL in optoelectronic devices.

Since the solid state structure of organic materials has a very important effect on their performance as interfacial layers in

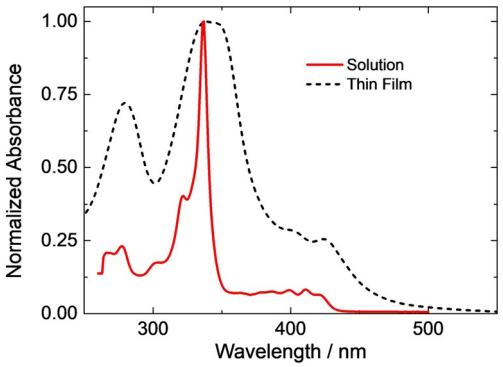

Figure 1. Normalized absorption spectra of **ADAI** in DMF solution (continuous line) and as thin film (dashed line).

optoelectronic devices, X-ray diffraction experiments have been employed to determine the crystal structure of **ADAI**. The structure of **ADAI** was solved ab initio by Simulated Annealing technique, followed by the refinement using the Rietveld method. The final Rietveld plot is shown in Figure S8 and the crystallographic parameters are summarized in Table S2 (Supporting Information). This compound crystallizes in the triclinic space group and possesses an essentially planar heptacyclic skeleton (Figure 2). Interestingly, the solid state packing exhibits the intended self-assembly directed by the hydrogen-bond donor and acceptor sites integrated in the polyheteroaromatic system. Each centrosymmetric molecule establishes four hydrogen bonds involving the nitrogen atoms of the pyridine rings and the NHs of the pyrrole rings, resulting in an ideal infinite lineal ribbon-like assembly (Figure 2a). Given the identical nature of the N–H···N contacts, all molecules display equidistant hydrogen bonds (2.9 Å, given as N···N distance). As can be seen in the expansion of the H-bonded ribbon projected through the molecular long axis (Figure 2b), molecules pack in very short steps of 0.66 Å defining an almost coplanar disposition. This arrangement is the consequence of self-assembled molecules further packing in a columnar mode (Figures 2b,c). The expansion of this π-stacked architecture shows how the hydrogen-bonded ribbon-like structure subsequently induces the piling-up of molecules, resulting in a highly ordered crystalline network (Figure 2d).

The use of ADAI as hole selective interlayer was tested in a *p*-i-n device architecture, employing $CH_3NH_3PbI_3$ as photoactive layer. A thin (≈10 nm) layer of **ADAI** was thermally evaporated on an ITO electrode, followed by deposition of $CH_3NH_3PbI_3$ as explained in the Experimental Section. The device was completed by depositing [60]PCBM as ETL and LiF and Al as back contact. PEDOT:PSS, commonly used in inverted perovskite solar cells, was used as reference. All details about the device fabrication can be found in the Experimental Section. The current density-voltage (*J-V*) characteristics measured using forward and reverse scans showed a good reproducibility and a small hysteresis (Figure S9 and Table S3, Supporting Information). In stabilized *J-V* scans, the best results obtained with PEDOT:PSS as HTL reached a short-circuit current density (J_{SC}) of 18.6 mA cm^{-2}, an open-circuit voltage (V_{OC}) of 1.00 V, and a fill factor (FF) of 0.73, resulting in a PCE of 13.8% (Table 1). Interestingly, the use of **ADAI** as interfacial layer, resulted in considerably enhanced overall device performance. The improvement in J_{SC} (19.4 mA cm^{-2}), V_{OC} (1.04 V), and FF (0.77) increased the PCE of the **ADAI**-based devices up to 15.5%. Device statistics (Table 1) confirm the improved performance of **ADAI** as HTL in *p*-i-n devices over PEDOT:PSS. Accordingly, **ADAI** is part of the selected group of highly efficient, undoped, neutral small molecular HTLs leading to a PCE over 15% in planar inverted $CH_3NH_3PbI_3$ perovskite solar cells.[25] External quantum efficien-

Table 1. Photovoltaic parameters of the perovskite solar cells under 1.5 AMG illumination in stabilized scans.

HTL	J_{SC} [mA cm^{-2}]	J_{SC}^{SR} [mA cm^{-2}][a]	V_{OC} [V]	FF	PCE [%]	PCE^{SR} [%][b]
PEDOT:PSS	18.6	17.0	1.00	0.73	13.8	12.4
ADAI	19.4	19.9	1.04	0.77	15.5	15.9

[a] Calculated by integration of the EQE spectrum with the AM1.5 G spectrum. [b] Based on J_{SC}^{SR}

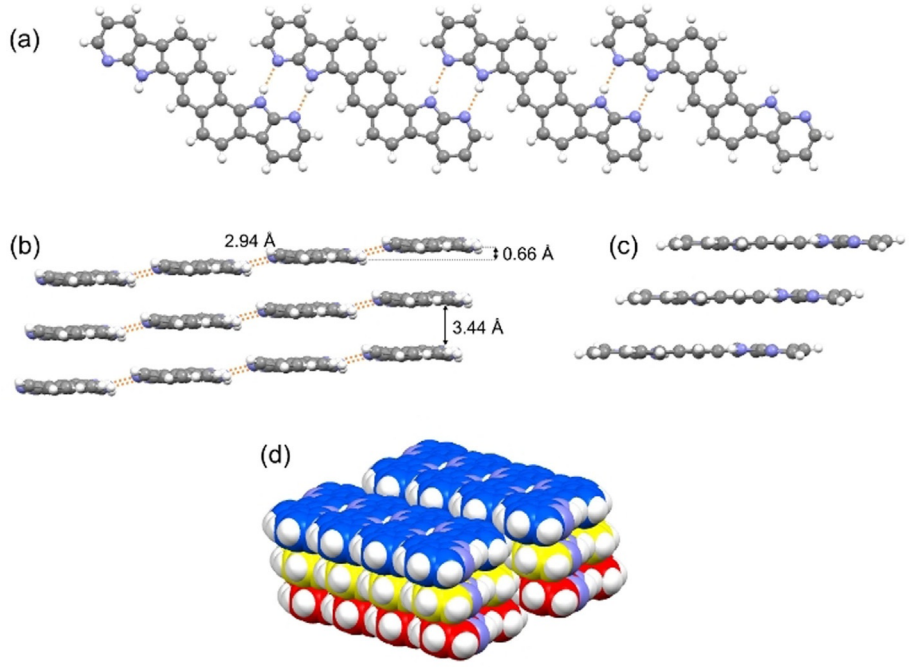

Figure 2. (a) Top view and (b) lateral view of the H-bonded ribbon-like structure of ADAI. Orange dotted lines represent the H-bond contacts. (c) Rotated lateral view showing the π–π stacking. (d) Expanded packing of hydrogen-bonded ribbon-like structures.

cy (EQE) spectra (Figure 3b) also evidence a better photon-to-electron conversion. For **ADAI** the EQE reaches a maximum value of 89.5% at 520 nm. The J_{SC}^{SR} values calculated from the integration of the EQE spectra with the 1.5 air mass solar spectrum (AM1.5G, 100 mW cm^{-2}) are within the accepted margin of error with those from the *J-V* characteristics, and refine the PCE value to 12.4 and 15.9% for the PEDOT:PSS and **ADAI** cells, respectively (Table 1). The photocurrent density and the PCE of devices fabricated with **ADAI** were monitored at the maximum power point ($V = 0.88$ V) under continuous illumination (Figure 3c). Both parameters remained stable for more than 1200 s with a variation of less than 1%.

To gain insight into the reasons for the improved performance with **ADAI**, the morphologies of the hole-transporting materials and the perovskite layer atop were examined by atomic force microscopy (AFM) and scanning electron microscopy (SEM). As can be seen in the AFM images of the HTMs deposited on ITO (Figure 4a,b) both materials formed rather smooth and homogenous layers. A low root-mean-square surface roughness (R_q) was determined for both PEDOT:PSS (R_q = 1.03 nm) and **ADAI** (R_q = 2.35 nm) on top of ITO and, according to the observed device performance of the *p*-i-n cells, these minor differences do not have a significant influence.

The properties of the subjacent hole-transport layer can drastically affect the nucleation and growth of the perovskite material during the crystallization process, which ultimately determines the performance of the solar cell.[26] In this regard, noticeable dissimilarities in the top morphology of the perovskite layers overlying the different HTLs (Figures 4c,d) were observed by SEM. Thus, $CH_3NH_3PbI_3$ perovskites grown on **ADAI** (Figure 4d) formed very compact films with larger crystalline domains and a reduced amount of pinholes and voids compared to those grown on PEDOT:PSS (Figure 4c) which presents a very similar morphology to that observed in previous reports for a hot casting deposition protocol.[23,27] The reduction of defects and grain boundaries in the perovskite layer reduces the chances for the photogenerated charges to become trapped and recombine, resulting in a concomitant improvement of the device performance.[28]

The efficiency of the charge transfer process at the perovskite/HTL interface was investigated by time-correlated single-photon counting (Figure 5). The PL decays revealed a decrease of the average PL lifetime ($\tau_{avg.}$, Table S4, Supporting Information) when comparing the neat perovskite film on glass (140.0 ns) to the perovskite deposited on PEDOT:PSS (114.7 ns) or **ADAI** (21.4 ns). These results suggest that the photogenerated charges in the perovskite active layers are extracted much faster when using **ADAI** as hole-transporting layer, which benefits the performance of the solar cell.

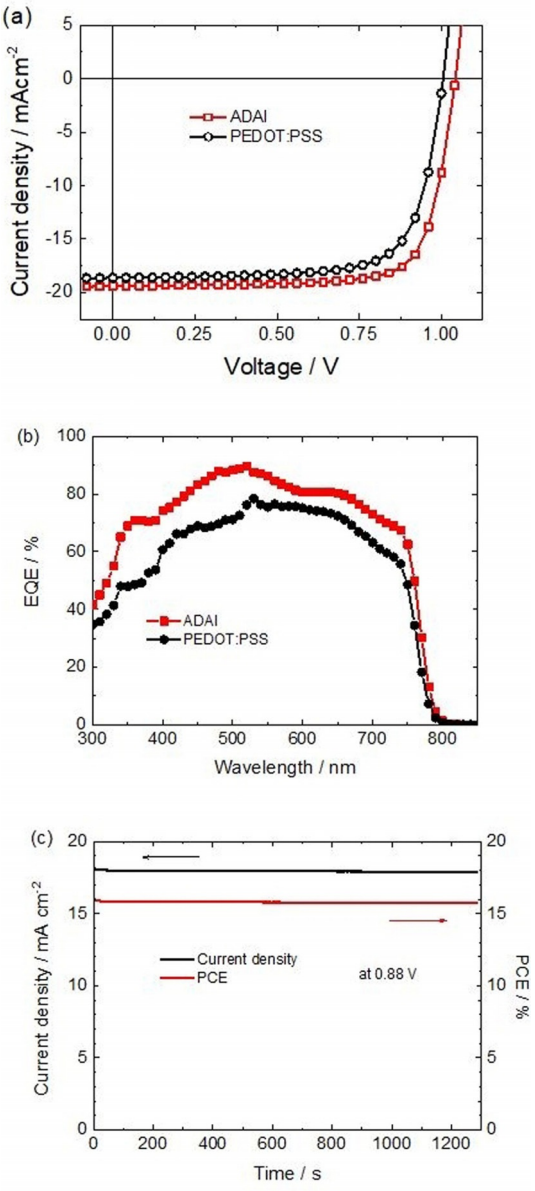

Figure 3. (a) Stabilized *J-V* characteristics of the optimized devices. (b) EQE spectra. (c) Current density and PCE of an **ADAI**-based device under constant illumination at the maximum power point vs. time.

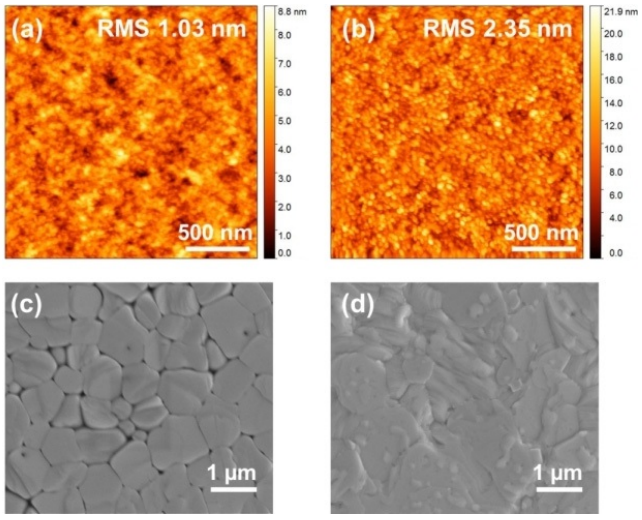

Figure 4. (a,b) Tapping mode AFM height images of the HTLs on ITO. Scan size: 2 µm × 2 µm. (c,d) Top view SEM images of the surface morphology of the $CH_3NH_3PbI_3$ perovskite films. (a,c) On ITO/PEDOT:PSS. (b,d) On ITO/**ADAI**.

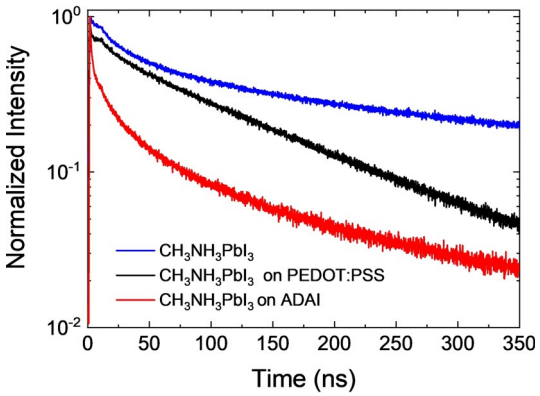

Figure 5. Time-resolved photoluminescence of $CH_3NH_3PbI_3$ layers on glass with and without HTL. Samples were photoexcited at 405 nm from the glass substrate side.

Charge recombination in photovoltaic materials limits the performance of a solar cell.[29] To understand the difference in photovoltaic performance for the two hole-transport layers (PEDOT:PSS vs. **ADAI**), we studied the extent of charge recombination by analyzing the effect of the incident light intensity on J_{SC} and V_{OC} using monochromatic light with two different wavelengths. Red light ($\lambda = 730$ nm) reaches a deeper section into the perovskite layer and enables the analysis of processes occurring in the bulk of the active layer, while blue light ($\lambda =$ 405 nm) is mainly absorbed close to the ITO/HTL/perovskite interface.[30] The light intensity dependence of the short-circuit current can generally be modeled by a power-law relationship:[31]

$$J_{SC} = C\Phi^{\alpha} \quad (1)$$

in which Φ denotes the photon flux, C is a constant, and α the exponent. Deviations from the ideal value ($\alpha = 1$) indicate non-optimal charge extraction. The α measured for the **ADAI** devices is very close to unity at both wavelengths ($\alpha_{red} = 1.004$; $\alpha_{blue} = 0.998$) (inset Figure 6a). On the other hand, the PEDOT:PSS-based devices show α values of 0.966 and 0.947 under illumination with red and blue light, respectively. Deviations from the ideal value can be better discerned in a plot of α vs. logΦ where α is calculated as $\log(J_{sc}/C)/\log\Phi$. Figure 6a shows that α of the **ADAI** based devices maintains a value very close to unity for both red and blue light over the whole intensity range.

The V_{OC} dependence on the light intensity is another diagnostic tool to investigate recombination mechanisms. The ideality factor, n_{id}, can be inferred by measuring V_{OC} as function of Φ using the expression:[32]

$$V_{OC} = \frac{E_g}{q} - \frac{n_{id}k_BT}{q}\ln\frac{\phi_0}{\phi} \quad (2)$$

Here E_g represents the band gap, q the elementary charge, k_B the Boltzmann constant, T the absolute temperature, and Φ_0 a constant with the same dimension as Φ. In general, two limiting scenarios are considered. For band-to-band recombination, $n_{id} = 1$ is expected, while for trap-assisted or Shockley-Read-Hall (SRH) recombination $n_{id} = 2$.[32] We studied the effect of the light intensity on the V_{OC} using red and blue light sources. For the cells with PEDOT:PSS as HTL the ideality factors

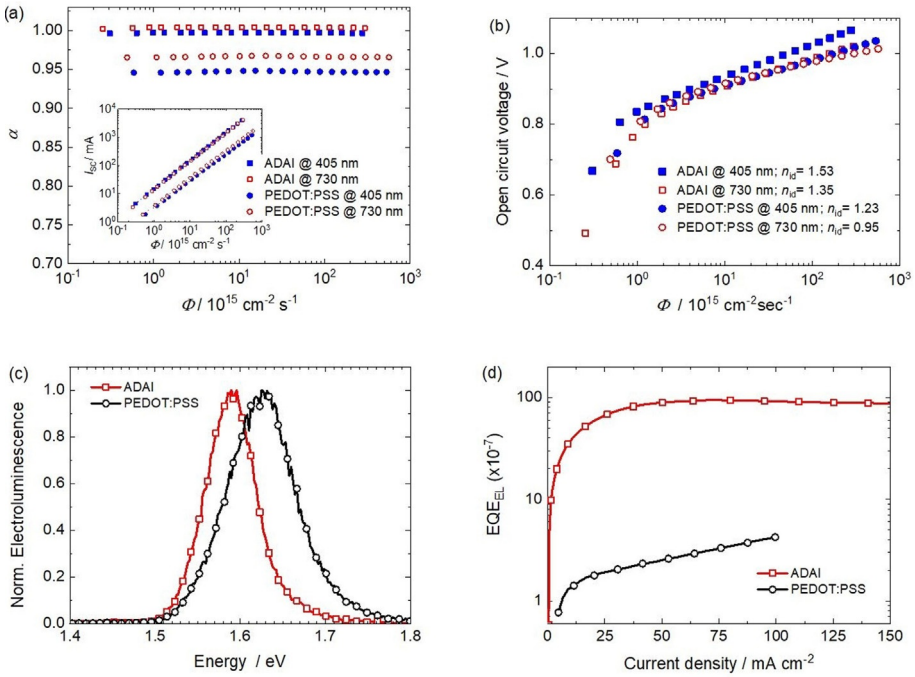

Figure 6. (a) Semi-logarithmic plot of α vs. Φ, inset: double-logarithmic plot of J_{SC} vs. Φ. (b) Open circuit voltage illuminating with wavelengths of 405 and 730 nm. Dashed lines correspond to the fittings. (c) Normalized electroluminescence spectra recorded at 1.2 V (d) External electroluminescence quantum efficiency (EQE_{EL}) as a function of the current density.

are low for both blue ($n_{id}=1.23$) and red ($n_{id}=0.95$) light (Figure 6b). In this case the low ideality factor is not beneficial, because also the V_{OC} is low. Such behavior has been observed previously for PEDOT:PSS based perovskite solar cells,[23,33] and can be related to surface recombination due to a non-selective contact or to the fact that the V_{OC} is limited by the built-in potential.[32,34] Devices fabricated with **ADAI** showed higher ideality factors of 1.35 and 1.53 for the red and blue light, respectively and higher V_{OC}, indicative of SRH recombination in the bulk in combination with band-to-band recombination.

With the aim of getting a better understanding of the recombination, we studied the electroluminescent (EL) properties. The normalized EL spectra recorded under forward bias (Figure 6c) reveal that optical band gaps, measured at the maximum of the EL,[35] are slightly different: $E_g=1.63$ eV for PEDOT:PSS and $E_g=1.59$ eV for **ADAI**. In addition, the full-width-at-half-maximum of the EL spectra is smaller for $CH_3NH_3PbI_3$ deposited on **ADAI** (67 meV) than on PEDOT:PSS (90 meV). The red shift observed for **ADAI** can be attributed to clustering and crystallization phenomena that result in larger perovskite grain sizes.[36] The narrower EL width for the **ADAI** device indicates that the electroluminescence originates from a more ordered distribution of states, presenting less defects in the perovskite semiconductor due to more crystalline order.

While radiative recombination is unavoidable in a solar cell, good performing photovoltaic devices should have little non-radiative recombination. For a $CH_3NH_3PbI_3$ perovskite with a band gap of 1.60 eV,[37] the radiative limit is $V_{OC,rad}\approx 1.31$ V.[35] As a result of non-radiative recombination, however, the measured open-circuit voltage in perovskite solar cells is often noticeably lower than the theoretical maximum attainable. The additional voltage loss due to non-radiative recombination ($\Delta V_{OC,nr}$) arises, amongst other causes, from defects (traps) either in the bulk of the material or at the interfacial regions. The non-radiative losses can be estimated from the external electroluminescence quantum efficiency (EQE_{EL}) measured for the solar cell operating in forward bias, according to the equation:[38]

$$V_{OC}=\frac{E_g}{q}-V_{OC,rad}-\Delta V_{OC,nr}=\frac{E_g}{q}-V_{OC,rad}-\frac{k_BT}{q}\ln\frac{1}{EQE_{EL}} \qquad (3)$$

Figure 6d shows that the EQE_{EL} achieved by devices incorporating **ADAI** as HTL is more than one order of magnitude higher than those measured for PEDOT:PSS. The non-radiative loss ($\Delta V_{OC,nr}$) estimated from the EQE_{EL} using Equation (3) is 0.32 V for **ADAI**. The V_{OC} predicted from the band gap and Equation (3) is then $\approx$0.98 V, in good agreement with the experimental value of 1.04 V. For the PEDOT:PSS device $\Delta V_{OC,nr}$ from the EQE_{EL} amounts to 0.40 V, but the larger loss is partly compensated by the wider band gap, such that the expected V_{OC} equals $\approx$0.94 V as compared to the experimental value of 1.00 V.

The difference of 0.04 V between the estimated V_{OC}s of the **ADAI** and PEDOT:PSS cells matches with the experimental result. We conclude that non-radiative recombination is reduced in devices employing **ADAI** as HTL compared to PEDOT:PSS. The results correlate well with those above observed for the J_{SC} dependence on light intensity, as well as to the previously discussed morphology of perovskite deposited on PEDOT:PSS, where smaller grains, pinholes and more extended grain boundaries are defects that can induce non-radiative recombination.[39]

Conclusions

In this contribution we report the synthesis and characterization of a novel centrosymmetric fused azapolyheteroaromatic molecule **ADAI** with an extended planar π-conjugated structure based on the fusion of two azaindole peripheral rings with an anthracene central moiety. When this new material is incorporated as hole-transporting layer in inverted $CH_3NH_3PbI_3$-based solar cells it provides a power conversion efficiency of 15.9% which approaches some of the best results reported for hole-transporting layers consisting in non-doped, small organic molecules in $CH_3NH_3PbI_3$ perovskite solar cells with a *p*-i-n device configuration. The success of **ADAI** as HTL, compared to the commonly used PEDOT:PSS, mainly relies on an improved perovskite layer morphology with reduced grain boundaries and larger crystalline domains, resulting in decreased non-radiative recombination losses and the reduction of undesired interfacial recombination mechanisms at the HTL/perovskite interface. Future work is directed towards tuning of the **ADAI** material design to possibly further improve the performance of this HTL for perovskite photovoltaics.

Acknowledgements

We thank C. Weijtens for performing the UPS measurements. Authors are grateful for the financial support from the Ministry of Science, Innovation and Universities (Project RTI2018-101092-B-I00), Fundación Séneca–Agencia de Ciencia y Tecnología de la Región de Murcia (Project 20959/PI/18 and M.M.-M. postdoctoral fellowship from "Saavedra Fajardo Program") and Programa Estatal de Fomento de la Investigación Científica y Técnica de Excelencia (RED2018-102815-T). P.G. acknowledges the University of Murcia for a FPU fellowship. Authors also acknowledge the Ministry of Science, Innovation and Universities and the Scientific Research Council (CSIC) for financial support and for provision of synchrotron radiation facilities, BM25-SpLine at the ERSF Synchrotron in Grenoble (France). This research has been further funded by the European Research Council under the European Union's Seventh Framework Programme (FP/2007–2013)/ ERC Grant Agreement No. 339031 and from the Ministry of Education, Culture and Science (Gravity program 024.001.035).

Conflict of interest

The authors declare no conflict of interest.

Keywords: fused-ring systems · organic electronics · self-assembly · solar cells · undoped hole-transport layer

[1] M. A. Green, A. Ho-Baillie, *ACS Energy Lett.* **2017**, *2*, 822.
[2] a) A. R. B. Mohd Yusoff, P. Gao, M. K. Nazeeruddin, *Coord. Chem. Rev.* **2018**, *373*, 258; b) M. L. Petrus, J. Schlipf, C. Li, T. P. Gujar, N. Giesbrecht, P. Müller-Buschbaum, M. Thelakkat, T. Bein, S. Hüttner, P. Docampo, *Adv. Energy Mater.* **2018**, *8*, 1703396; c) Q. Lin, Z. Wang, H. J. Snaith, M. B. Johnston, L. M. Herz, *Adv. Sci.* **2018**, *5*, 1700792; d) J.-P. Correa-Baena, M. Saliba, T. Buonassisi, M. Grätzel, A. Abate, W. Tress, A. Hagfeldt, *Science* **2017**, *358*, 739.
[3] S. De Wolf, J. Holovsky, S.-J. Moon, P. Löper, B. Niesen, M. Ledinsky, F.-J. Haug, J.-H. Yum, C. Ballif, *J. Phys. Chem. Lett.* **2014**, *5*, 1035.
[4] G. Xing, N. Mathews, S. Sun, S. S. Lim, Y. M. Lam, M. Grätzel, S. Mhaisalkar, T. C. Sum, *Science* **2013**, *342*, 344.
[5] C. Wehrenfennig, G. E. Eperon, M. B. Johnston, H. J. Snaith, L. M. Herz, *Adv. Mater.* **2014**, *26*, 1584.
[6] S. D. Stranks, G. E. Eperon, G. Grancini, C. Menelaou, M. J. P. Alcocer, T. Leijtens, L. M. Herz, A. Petrozza, H. J. Snaith, *Science* **2013**, *342*, 341.
[7] W.-J. Yin, T. Shi, Y. Yan, *Appl. Phys. Lett.* **2014**, *104*, 063903.
[8] a) J. S. Manser, J. A. Christians, P. V. Kamat, *Chem. Rev.* **2016**, *116*, 12956; b) J. Huang, Y. Yuan, Y. Shao, Y. Yan, *Nat. Rev. Mater.* **2017**, *2*, 17042; c) T. M. Brenner, D. A. Egger, L. Kronik, G. Hodes, D. Cahen, *Nat. Rev. Mater.* **2016**, *1*, 15007; d) V. Adinolfi, W. Peng, G. Walters, O. M. Bakr, E. H. Sargent, *Adv. Mater.* **2018**, *30*, 1700764.
[9] National Renewable Energy Laboratory, N.R.E.L. https://www.nrel.gov/pv/assets/pdfs/pv-efficiencies-07 – 17 – 2018.pdf.
[10] a) M. Saliba, J.-P. Correa-Baena, C. M. Wolff, M. Stolterfoht, N. Phung, S. Albrecht, D. Neher, A. Abate, *Chem. Mater.* **2018**, *30*, 4193; b) Z. Li, T. R. Klein, D. H. Kim, M. Yang, J. J. Berry, M. F. A. M. van Hest, K. Zhu, *Nat. Rev. Mater.* **2018**, *3*, 18017.
[11] J. A. Christians, S. N. Habisreutinger, J. J. Berry, J. M. Luther, *ACS Energy Lett.* **2018**, *3*, 2136.
[12] a) M. M. Lee, J. Teuscher, T. Miyasaka, T. N. Murakami, H. J. Snaith, *Science* **2012**, *338*, 643; b) P. Docampo, J. M. Ball, M. Darwich, G. E. Eperon, H. J. Snaith, *Nat. Commun.* **2013**, *4*, 2761; c) J.-Y. Jeng, Y.-F. Chiang, M.-H. Lee, S.-R. Peng, T.-F. Guo, P. Chen, T.-C. Wen, *Adv. Mater.* **2013**, *25*, 3727.
[13] a) T. Liu, K. Chen, Q. Hu, R. Zhu, Q. Gong, *Adv. Energy Mater.* **2016**, *6*, 1600457; b) Y. Bai, X. Meng, S. Yang, *Adv. Energy Mater.* **2018**, *8*, 1701883.
[14] A. Rajagopal, K. Yao, A. K.-Y. Jen, *Adv. Mater.* **2018**, *30*, 1800455.
[15] a) E. J. Juarez-Perez, M. Wuβler, F. Fabregat-Santiago, K. Lakus-Wollny, E. Mankel, T. Mayer, W. Jaegermann, I. Mora-Sero, *J. Phys. Chem. Lett.* **2014**, *5*, 680; b) C. Rodríguez-Seco, L. Cabau, A. Vidal-Ferran, E. Palomares, *Acc. Chem. Res.* **2018**, *51*, 869.
[16] a) W. Yan, S. Ye, Y. Li, W. Sun, H. Rao, Z. Liu, Z. Bian, C. Huang, *Adv. Energy Mater.* **2016**, *6*, 1600474; b) X. Zhao, M. Wang, *Mater. Today Energy* **2018**, *7*, 208.
[17] a) M. P. de Jong, L. J. van Ijzendoorn, M. J. A. de Voigt, *Appl. Phys. Lett.* **2000**, *77*, 2255; b) T. Liu, F. Jiang, F. Qin, W. Meng, Y. Jiang, S. Xiong, J. Tong, Z. Li, Y. Liu, Y. Zhou, *ACS Appl. Mater. Interfaces* **2016**, *8*, 33899.
[18] a) P. Gómez, S. Georgakopoulos, J. P. Cerón, I. da Silva, M. Más-Montoya, J. Pérez, A. Tárraga, D. Curiel, *J. Mater. Chem. C* **2018**, *6*, 3968; b) P. Gómez, M. Más-Montoya, I. da Silva, J. P. Cerón-Carrasco, A. Tárraga, D. Curiel, *Cryst. Growth Des.* **2017**, *17*, 3371.
[19] S. Kuster, T. Geiger, *Dyes Pigm.* **2015**, *113*, 110.
[20] a) P. Ruiz-Castillo, S. L. Buchwald, *Chem. Rev.* **2016**, *116*, 12564; b) S. Wagaw, S. L. Buchwald, *J. Org. Chem.* **1996**, *61*, 7240.
[21] M. E. Budén, V. A. Vaillard, S. E. Martin, R. A. Rossi, *J. Org. Chem.* **2009**, *74*, 4490.
[22] M. L. Petrus, T. Bein, T. J. Dingemans, P. Docampo, *J. Mater. Chem. A* **2015**, *3*, 12159.
[23] B. J. Bruijnaers, E. Schiepers, C. H. L. Weijtens, S. C. J. Meskers, M. M. Wienk, R. A. J. Janssen, *J. Mater. Chem. A* **2018**, *6*, 6882.
[24] J. C. Blakesley, F. A. Castro, W. Kylberg, G. F. A. Dibb, C. Arantes, R. Valaski, M. Cremona, J. S. Kim, J.-S. Kim, *Org. Electron.* **2014**, *15*, 1263.
[25] a) H. Chen, W. Fu, C. Huang, Z. Zhang, S. Li, F. Ding, M. Shi, C.-Z. Li, A. K. Y. Jen, H. Chen, *Adv. Energy Mater.* **2017**, *7*, 1700012; b) C. Huang, W. Fu, C.-Z. Li, Z. Zhang, W. Qiu, M. Shi, P. Heremans, A. K. Y. Jen, H. Chen, *J. Am. Chem. Soc.* **2016**, *138*, 2528; c) Y. Li, Z. Xu, S. Zhao, B. Qiao, D. Huang, L. Zhao, J. Zhao, P. Wang, Y. Zhu, X. Li, X. Liu, X. Xu, *Small* **2016**, *12*, 4902; d) S. J. Park, S. Jeon, I. K. Lee, J. Zhang, H. Jeong, J.-Y. Park, J. Bang, T. K. Ahn, H.-W. Shin, B.-G. Kim, H. J. Park, *J. Mater. Chem. A* **2017**, *5*, 13220; e) L. Yang, F. Cai, Y. Yan, J. Li, D. Liu, A. J. Pearson, T. Wang, *Adv. Funct. Mater.* **2017**, *27*, 1702613; f) J. Zhang, Q. Sun, Q. Chen, Y. Wang, Y. Zhou, B. Song, N. Yuan, J. Ding, Y. Li, *Adv. Funct. Mater.* **2019**, *29*, 1900484; g) B. Wang, Q. Zeng, Z. Sun, S. Xue, M. Liang, *Dyes Pigm.* **2019**, *165*, 81; h) Y. Chen, X. Xu, N. Cai, S. Qian, R. Luo, Y. Huo, S.-W. Tsang, *Adv. Energy Mater.* **2019**, *9*, 1901268.
[26] T. Geske, J. Li, M. Worden, X. Shan, M. Chen, S. G. R. Bade, Z. Yu, *Adv. Funct. Mater.* **2017**, *27*, 1702180.
[27] J. J. van Franeker, K. H. Hendriks, B. J. Bruijnaers, M. W. G. M. Verhoeven, M. M. Wienk, R. A. J. Janssen, *Adv. Energy Mater.* **2017**, *7*, 1601822.
[28] a) R. Long, J. Liu, O. V. Prezhdo, *J. Am. Chem. Soc.* **2016**, *138*, 3884; b) J.-P. Correa-Baena, M. Anaya, G. Lozano, W. Tress, K. Domanski, M. Saliba, T. Matsui, T. J. Jacobsson, M. E. Calvo, A. Abate, M. Grätzel, H. Míguez, A. Hagfeldt, *Adv. Mater.* **2016**, *28*, 5031; c) X. Ren, Z. Yang, D. Yang, X. Zhang, D. Cui, Y. Liu, Q. Wei, H. Fan, S. Liu, *Nanoscale* **2016**, *8*, 3816.
[29] a) J. Chen, N.-G. Park, *Adv. Mater.* **2019**, *31*, 1803019; b) L. Contreras-Bernal, M. Salado, A. Todinova, L. Calio, S. Ahmad, J. Idígoras, J. A. Anta, *J. Phys. Chem. C* **2017**, *121*, 9705.
[30] J.-P. Correa-Baena, W. Tress, K. Domanski, E. H. Anaraki, S.-H. Turren-Cruz, B. Roose, P. P. Boix, M. Grätzel, M. Saliba, A. Abate, A. Hagfeldt, *Energy Environ. Sci.* **2017**, *10*, 1207.
[31] a) L. J. A. Koster, V. D. Mihailetchi, H. Xie, P. W. M. Blom, *Appl. Phys. Lett.* **2005**, *87*, 203502; b) S. R. Cowan, A. Roy, A. J. Heeger, *Phys. Rev. B* **2010**, *82*, 245207.
[32] W. Tress, M. Yavari, K. Domanski, P. Yadav, B. Niesen, J. P. Correa Baena, A. Hagfeldt, M. Graetzel, *Energy Environ. Sci.* **2018**, *11*, 151.
[33] a) K. Tvingstedt, L. Gil-Escrig, C. Momblona, P. Rieder, D. Kiermasch, M. Sessolo, A. Baumann, H. J. Bolink, V. Dyakonov, *ACS Energy Lett.* **2017**, *2*, 424; b) W. Tress, *Adv. Energy Mater.* **2017**, *7*, 1602358.
[34] S. Solak, P. W. M. Blom, G. A. H. Wetzelaer, *Appl. Phys. Lett.* **2016**, *109*, 053302.
[35] K. Tvingstedt, O. Malinkiewicz, A. Baumann, C. Deibel, H. J. Snaith, V. Dyakonov, H. J. Bolink, *Sci. Rep.* **2014**, *4*, 6071.
[36] a) V. D'Innocenzo, A. R. Srimath Kandada, M. De Bastiani, M. Gandini, A. Petrozza, *J. Am. Chem. Soc.* **2014**, *136*, 17730; b) S. Mastroianni, F. D. Heinz, J. H. Im, W. Veurman, M. Padilla, M. C. Schubert, U. Würfel, M. Grätzel, N. G. Park, A. Hinsch, *Nanoscale* **2015**, *7*, 19653.
[37] S. Rühle, *Sol. Energy* **2016**, *130*, 139.
[38] a) S. D. Stranks, *ACS Energy Lett.* **2017**, *2*, 1515; b) W. Tress, N. Marinova, O. Inganäs, M. K. Nazeeruddin, S. M. Zakeeruddin, M. Graetzel, *Adv. Energy Mater.* **2015**, *5*, 1400812.
[39] T. S. Sherkar, C. Momblona, L. Gil-Escrig, J. Ávila, M. Sessolo, H. J. Bolink, L. J. A. Koster, *ACS Energy Lett.* **2017**, *2*, 1214.

Manuscript received: January 1, 2020
Accepted manuscript online: March 4, 2020
Version of record online: July 1, 2020